PCCP

ROYAL SOCIETY OF CHEMISTRY

PAPER

View Article Online
View Journal | View Issue

Cite this: *Phys. Chem. Chem. Phys.*, 2026, **28**, 7645

Probing the photoabsorption features and electronic excited states of propylene oxide: an experimental and theoretical study

Mónica Mendes, *[a] João Ameixa, [ab] Rodrigo Rodrigues, [a] Diogo Sequeira, [a] Nykola C. Jones, [c] Søren V. Hoffmann, [c] Alessandra Souza Barbosa *[d] and Filipe Ferreira da Silva [a]

Propylene oxide is the first chiral molecule identified in the interstellar medium, which has resulted in growing interest in it as a prototypical molecule to study the origin of life on Earth. Numerous spectroscopic studies have investigated the excitation, ionization and dissociation of propylene oxide by photons, electrons and/or ions. However, for vacuum ultraviolet (VUV) photoabsorption spectroscopy, data are available only for energies between 6 and 9 eV with low energy resolution. Here, we present the high-resolution VUV photoabsorption cross-sections in the 6.0–10.8 eV range through an experimental and theoretical approach. The measurements were carried out using a VUV synchrotron radiation light source and are supported by quantum chemical calculations performed using time-dependent density functional theory. There is good agreement between experiment and theory, allowing us to characterize the main absorption bands assigned to electronic transitions involving mainly oxygen lone pairs and lower-lying Rydberg states. At higher energy, there are several Rydberg states observable, characterized by superimposed features with different vibrational progressions. Some features observed in the spectrum are assigned to vibrational modes involving the methyl group, namely CH_3 bending (υ_{22} and υ_{23}) and CH_3 torsion (υ_{24}). Additionally, we report a vibrational progression which may be related to the cation ring CC stretching with an average frequency of about 565 cm^{-1}. Calculated potential energy curves for the low-lying excited states along the C–CH_3 stretching coordinate reveal that the initial Rydberg states evolve into dissociative states at larger bond distances, as the σ* valence character increases.

Received 5th January 2026,
Accepted 19th February 2026

DOI: 10.1039/d6cp00031b

rsc.li/pccp

A. Introduction

Chirality was defined by Vladimir Prelog in his Nobel Prize lecture in 1975 as "An object is chiral if it cannot be brought into congruence with its mirror image by translation and rotation".[1] Chiral homogeneity is a characteristic found in living systems, structures and functions.[2,3] The question "why do only L-enantiomers of amino acids occur in proteins, and D-sugars in nucleic acids?" remains unresolved. This characteristic is essential to define the structural integrity and functions of biopolymers, as well as being key to many metabolism reactions, which are features of life on Earth.[3,4] The explanation for this selection by terrestrial organisms could rely on racemic mixtures of chiral molecules synthesized in the interstellar medium (ISM), where an enantiomer is preferentially photolyzed by UV-polarized photons or low energy spin polarized secondary electrons, or subjected to asymmetric beta-decay-linked radiolysis.[5,6] For example, some prebiotic molecules, such as cyanomethanimine (NC_2HNH), which is a precursor of the adenine DNA nucleobase, are formed in the ISM through mechanisms initiated by high-energy cosmic ray particles and ionizing photons.[7] Amino acids, such as alanine,[8,9] glutamic acid[10] and leucine,[11] were also intensively studied, making use of VUV-circularly polarized light (VUV-CPL) and showed enantioselectivity *via* photolysis. Clusters of L-serine have shown extreme homochirality prevalence when exposed to electrons under helium nanodroplet conditions.[12] These results are highly remarkable considering the detection of interstellar gases such as propylene oxide and glycine in star-forming regions.[4]

[a] *CEFITEC, Departamento de Física, NOVA School of Science and Technology, Universidade NOVA de Lisboa, 2829-516 Caparica, Portugal. E-mail: mf.mendes@fct.unl.pt*
[b] *Portuguese Navy Research Center (CINAV), Portuguese Naval Academy (Escola Naval), Almada, 2810-001, Portugal*
[c] *ISA, Department of Physics and Astronomy, Aarhus University, Ny Munkegade 120, 8000 Aarhus C, Denmark*
[d] *Departamento de Física, Universidade Federal do Paraná, Caixa Postal 19044, Curitiba 81531-980, PR, Brazil. E-mail: alessandra@fisica.ufpr.br*

In the ISM, the production of simple molecules, such as CO, CN, water or ammonia, and even small molecules such as formamide ($HCONH_2$), a potential precursor for genetic and metabolic molecules, is dominated by gas phase reactions. On the other hand, more complex saturated organic molecules, known as prebiotic compounds, are found in bare dust grains, or in ice mantles.[5] Even though these are very low temperature environments, gas phase reactions may play a role in the chain of events of adsorption and desorption, also being involved in the formation of complex molecular entities existing in the ISM.

Propylene oxide (CH_3CHOCH_2), also referred to as methyloxirane or epoxypropane, is the first chiral molecule detected outside the solar system using data from the available Prebiotic Interstellar Molecular Survey (PRIMOS) project at the Green Bank Telescope (GBT). It was identified in 2016, in the gas phase, towards the high-mass star-forming region Sagittarius B2(N) molecular cloud.[13] The recent detection of racemic propylene oxide in the ISM has become an important pathway to better understand the origin of enantiomeric excesses, which subsequently allow us to elucidate the emergence of homochirality on life on Earth. Bergantini *et al.*[6] reported, through a combined theoretical and experimental study, the first steps in the synthesis of propylene oxide in the ISM *via* non-equilibrium chemistry triggered by secondary electrons generated in the track of cosmic rays interacting with ice-coated interstellar grains through excited-state and spin-forbidden reaction pathways. Also, several researchers have investigated propylene oxide on a fundamental molecular physics basis to obtain insights into ionization, dissociation and vibrational excitation phenomena. Appearance potentials and relative abundances for the main cations produced from electron ionization of propylene oxide were studied by Gallegos and Kiser,[14] and more recently, by Rodrigues *et al.*,[15] as well as through mass-resolved photoionization spectroscopy by Liu *et al.*[16] Both researchers also reported potential reaction pathways computed through quantum chemical calculations. An early 1980s study on the unimolecular decay of the propylene oxide cation was also conducted *via* photoelectron-photoion coincidence spectroscopy.[17] That work showed that the propylene oxide cation is initially formed with no or only little vibrational excitation in the electronic ground state, presenting a non-dissociative character and a similar geometry of the neutral ground state.[17] Additionally, stable $C_3H_6O^+$ ions were observed within the energy range of the $2^+(\tilde{\chi})$ state (<10.5 eV). The first ionization energy of propylene oxide has been reported by several groups in the range 9.80–10.44 eV, with the spread largely reflecting whether adiabatic or vertical values are reported.[14–16,18,19] The vibrational spectrum of propylene oxide was experimentally obtained by M. C. Tobin[20] and Polavarapu *et al.*[21] in the early 1960s and 1980s, respectively. More recently, the molecular structure, vibrational harmonic and anharmonic frequencies and infrared (IR) spectrum of the propylene oxide ground electronic state were analysed by Barone *et al.*[22] Additionally, propylene oxide has been extensively studied by different gas phase experiments, such as high-resolution IR spectroscopy and rovibrational analysis of the υ_{12} band,[23] vibrational circular dichroism (VCR),[24] ultraviolet circular dichroism,[25] microwave spectrum,[26] circular dichroism in photoelectron spectroscopy,[27,28] as well as by *ab initio* quantum calculations.[29–35] As far as we know, there are two previous experimental investigations on the electronic excited states of gas phase propylene oxide reported by Breest *et al.*[36] and Cohen *et al.*[37] through vacuum ultraviolet (VUV) spectroscopy for energies from 6.5 eV up to 9 eV.

Here, we report a combined experimental and theoretical study on the high-resolution VUV photoabsorption of gas phase propylene oxide in the 6.0–10.8 eV photon energy range. We present and discuss the main absorption bands, the assignments of the excited states and the corresponding vibrational progressions, supported by time-dependent density functional theory (TDDFT) calculations. This represents a comprehensive study of the excited states of propylene oxide and could shed further light on the subsequent production of radicals and ions, which could bring forth information on its role in ISM chemistry.

B. Methods

B.1. Experimental methods

The high-resolution VUV photoabsorption spectrum of propylene oxide was measured using the AU-UV beam line of the ASTRID2 storage ring facility at Aarhus University in Denmark. The full description of the experimental apparatus can be found in a previous publication.[38] Briefly, the setup comprises a gas cell coupled to a monochromator with a MgF_2 window, which separates it from the ultrahigh vacuum (UHV) of the beamline. The transmitted light intensity is detected by a photomultiplier tube (PMT) after the interaction of synchrotron radiation with a static gas sample. A capacitance manometer (Chell CDG100D) is used to record the absolute pressure of the effusive molecular gas. The wavelength is selected using a toroidal dispersion grating with 2000 lines per mm providing a resolution of 0.075 nm, corresponding to 3 meV at the midpoint of the present energy range. The full wavelength range of the monochromator is calibrated through the measurement of fine peaks for nitrogen and sulphur dioxide, with an accuracy of ± 0.05 nm. To avoid any absorption of O_2 from the air, for energies above 6.20 eV (200 nm), there is a small gap between the PMT and the MgF_2 gas cell exit window, which is evacuated using a scroll pump. For higher wavelength measurements, air is admitted into the gap at atmospheric pressure to allow O_2 to absorb any higher orders of light produced by the monochromator. Absolute photoabsorption cross-sections (σ) were obtained at room temperature (~ 25 °C) by using the Beer–Lambert attenuation law $I_t = I_0 \exp(-N\sigma l)$, where I_t is the light intensity transmitted through the gas sample, I_0 is the intensity transmitted through the evacuated cell, N is the molecular density, and l is the absorption path length (15.5 cm). The measurements were taken over a range of pressures between 0.04 and 1.3 mbar, ensuring that the

attenuation remained low enough to avoid saturation effects. The spectrum was measured in the energy range from 5.635 eV (220 nm) to 10.781 eV (115 nm) using data points separated by 0.05 nm (Fig. 1). The accuracy of the cross-sections is estimated to be ~10%, which is ensured by recording the VUV spectra in small (5 or 10 nm) sections to allow optimization of pressure according to the local cross-sections, with at least 10 data points overlapping between the adjoining ranges.[38] The VUV photoabsorption spectrum was taken at room temperature and, since the vapour pressure of the gas was extremely high, there were no problems obtaining higher pressures which allow for accurate measurement of low cross-section features. The reproducibility of the spectrum was confirmed through repeated measurements of each region, ensuring a good overlap between adjoining ranges and with a broad scan taken in larger step sizes. The racemic propylene oxide sample (CAS: 75-56-9) was purchased from Sigma-Aldrich with a stated purity of ≥99.5%. The sample was used without further purification and degassed before measurement through repeated freeze–pump–thaw cycles.

B.2. Theoretical methods

All calculations were carried out using the GAMESS-US package.[39] Initially, the molecular geometry was optimized at the density functional theory (DFT) level, using the CAMB3LYP functional and the aug-cc-pVQZ basis set. Harmonic vibrational frequency analyses confirmed the stationary point as a true minimum. The vertical excitation energies and oscillator strengths were obtained at time-dependent DFT using the same functional and basis set. The molecular orbitals (MOs), as obtained in the TDDFT/CAMB3LYP/aug-cc-pVQZ calculations, are shown in the SI together with the full table showing the most dominant transitions in each excitation energy. Since most electronic excitations are described by more than one pair of occupied and unoccupied MOs, we have also carried out natural transition orbital (NTO) analyses to characterize the electronic nature of the transitions and make the discussion more straightforward. Additional calculations with different functional and basis sets were also carried out and are available in the SI.

We also obtained calculated photoabsorption cross-sections, obtained in the vertical approximation, by convoluting the calculated oscillator strengths with Gaussian functions of 0.3 eV full width at half maximum (FWHM). This value was chosen to provide the best comparison with the experimental data. In the SI we also show the calculated cross-sections obtained with different functionals and/or basis sets.

Additionally, potential energy curve calculations were carried out along the C–CH_3 stretching coordinate at the TDDFT/CAMB3LYP/aug-cc-pVQZ level. The excitation energies were obtained by rigidly scanning the selected bond length while keeping all other internal coordinates fixed at their ground-state equilibrium values. This approach allows for a direct assessment of how bond elongation influences the electronic character of the excited states and facilitates identification of Rydberg–valence mixing effects.

It is worth mentioning that the C–CH_3 coordinate was chosen as a representative distortion to probe Rydberg–valence mixing effects and is not intended to represent a specific or dominant photodissociation pathway. To provide insights into the relevance of C–O bond elongation and the potential of ring-opening pathways, additional potential energy scans were also performed along each inequivalent C–O stretching coordinate. These supplementary calculations were carried out at the TDDFT/CAM-B3LYP/aug-cc-pVTZ level and are reported in the SI.

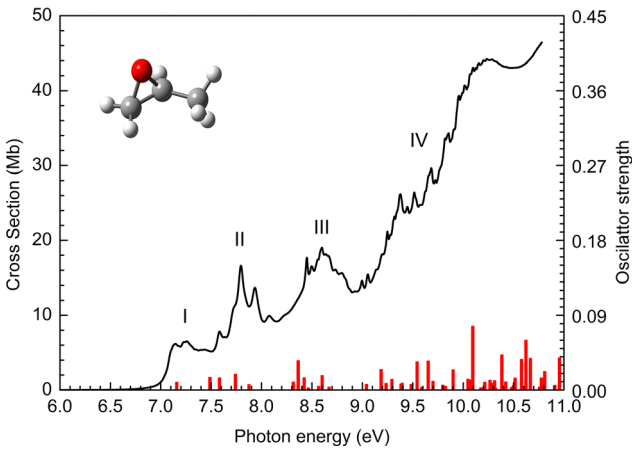

Fig. 1 High-resolution VUV photoabsorption cross-section of propylene oxide (black line) and calculated excitation energies and oscillator strengths (red bars) at the TDDFT/CAMB3LYP/aug-cc-pVQZ level. The four bands discussed in the text are also labelled in the figure.

C. Results and discussion

Propylene oxide belongs to the C1 point group and, therefore, all dipole transitions are allowed. The outermost molecular orbitals are ... $(13a)^2$ $(14a)^2$ $(15a)^2$ $(16a)^2$. The highest occupied molecular orbital (HOMO) corresponds primarily to the oxygen lone-pair (n_O), whereas HOMO−1, HOMO−2 and HOMO−3 are predominantly assigned as σ_{CO}, σ_{CH}/n_O, and σ_{CC}/n_O, respectively. Most of the calculated transitions are initiated in these occupied orbitals.

Fig. 1 shows the experimental high-resolution VUV photoabsorption spectrum from 6.0 to 10.8 eV photon energy, compared with the calculated oscillator strengths (f_0). The spectrum is divided into four main absorption bands, and several fine features were resolved. The computed photoabsorption cross-section is presented in Fig. 2, where it is compared with the experimental results. We found a reasonably good agreement between theoretical and experimental data, which allows us to interpret the measured absorption bands based on the quantum chemical calculations. As mentioned earlier, the assignments of calculated transitions are based on NTO analysis, with typical NTOs shown in Fig. 3. Although the specific NTOs differ from state to state, overall, they present similar qualitative features. In particular, the typically occupied NTOs

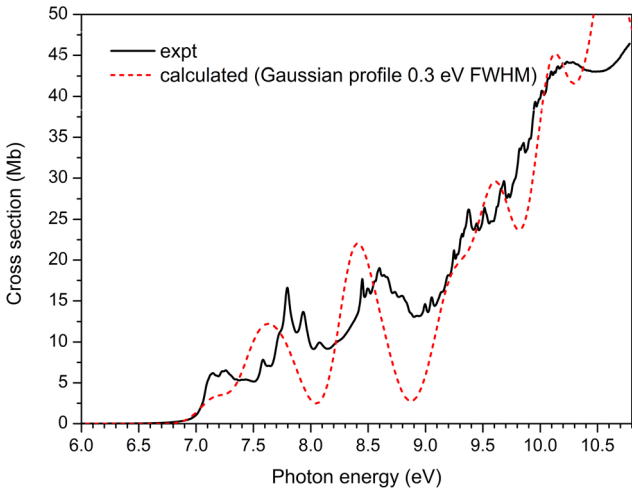

Fig. 2 Comparison between the experimental (black) and calculated (red) photoabsorption cross-sections of propylene oxide, obtained in the vertical approximation, with a Gaussian profile.

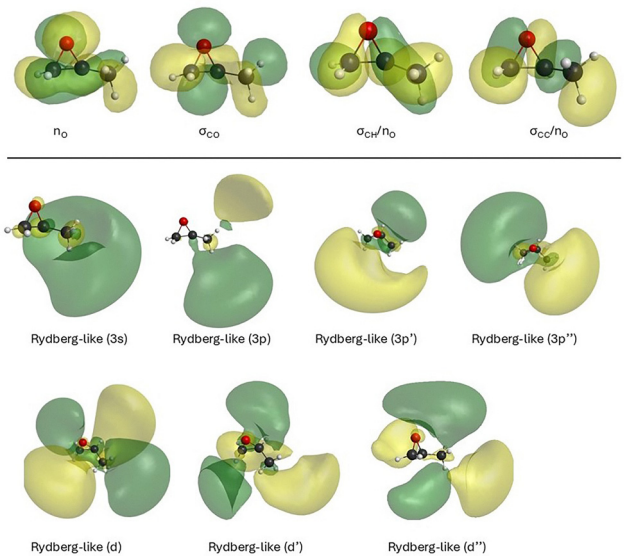

Fig. 3 Typical hole and particle NTOs involved in the low-lying electronic transitions of propylene oxide.

are closely related to the HOMO, HOMO−1, HOMO−2 and HOMO−3. The dominant transitions are mainly assigned to electronic excitations to Rydberg-like orbitals, of s, p and d type. Table 1 summarizes the computed vertical excitation energies, oscillator strengths and major assignments of the electronically excited states of propylene oxide, together with the experimental energies and respective cross section values for each absorption band (I to IV).

We have also proposed vibrational assignments based on the orbitals involved in the dominant excitations, the character of the vibrational modes as well as the identification of a given progression in the spectrum. The vibrational modes nomenclature follows that presented in ref. 21 and reported in Table S3, also with the computed vibrational frequencies.

The Rydberg states – characterized by excitation into diffuse (Rydberg) orbitals – were also obtained for the ionic electronic ground (IE_1) and first excited (IE_2) states and are presented in Table 2. The two lowest experimental vertical ionization energies (IEs) of 10.26 and 11.23 eV[17] were used to estimate the Rydberg series using the well-known Rydberg formula, E_n = IE − $(13.61/(n-\delta)^2)$ (eV), where the excitation energy E_n is estimated from the ionization energy IE, the principal quantum number n, and the quantum defect δ. Due to the character of the orbitals for the main dominant transitions (Fig. 3), it is expected that the VUV photoabsorption spectrum of propylene oxide is significantly influenced by the Rydberg states, and subsequent identification of Rydberg progressions. This will be described and discussed in detail in the following sections where energy ranges are loosely defined.

C.1. The 6.7–7.5 eV photon energy range (band I)

The first and lowest intensity band is centred at 7.26 eV with a cross-section maximum of 6.5 Mb. According to our TDDFT calculations, there is only one state for this band at 7.16 eV, with f_0 = 0.001. The NTO analysis of this state assigns this transition to the promotion of an electron from the oxygen lone-pair orbital to the Rydberg-like 3s orbital ($n_O \rightarrow 3s$). This band is the lowest intensity band in the overall energy spectrum, and it is possible to identify two vibrational progressions involving the CH_3 group. The 0–0 transition of propylene oxide is tentatively placed at 7.10 eV, which is followed by a clear vibrational progression with a spacing of around 0.02 eV, assigned to the υ_{24} CH_3 torsion. The υ_{23} CH_3 bending vibrational mode is also identified with an energy spacing of 0.04 eV (Table 3). Our rationale for these assignments is based on the vibrational energy of these modes, υ_{24} CH_3 torsion and υ_{23} CH_3 bend, which are 0.025 eV and 0.046 eV, respectively and, therefore, matching our results (Table S3). Moreover, both modes are dominated by the vibration of the CH_3 group, which would be expected to be activated based on the orbitals involved in this electronic excitation (Fig. 3). In Fig. 2, we also compare the measured and calculated cross sections of propylene oxide, the latter obtained in the vertical approximation. There is good agreement between both spectra in the 6.7–7.5 energy range, where the major discrepancy resides in the intensity of the band, with the calculated cross-section values being slightly below the experimental values. Previous works by Breest *et al.*[36] and Cohen *et al.*[37] have also reported an electronic transition $n_O \rightarrow R(3s)$ at 7.08 eV and 7.12 eV, respectively. This is in accordance with our results with redshifts of 0.18 eV and 0.14 eV, respectively. Here, the major difference relies on the spectral resolution between the three studies. In our and Breest *et al.*[36] spectra, the resolution allows us to distinguish two main structures and even, in our case, vibrational progressions, which are not observed by Cohen *et al.*[37]

According to the quantum defect analysis, it is expected that a 3s Rydberg progression is starting at 7.15 eV with a quantum defect of 0.91 converging to the ionic electronic ground state (IE_1) of 10.26 eV (Table 2 and Fig. 4), in good agreement with

Table 1 Calculated vertical excitation energies (ΔE), in eV, vertical oscillator strengths (f_0), and character (based in the NTO analysis, of propylene oxide, computed at the TDDFT/CAMB3LYP/aug-cc-pVQZ level of theory, compared with the experimentally obtained band maxima, in eV, and peak cross-section, in Mb. When the Rydberg orbital type could not be uniquely determined, the virtual orbital was labeled as "Ryd-like"

Experimental			Theoretical		
Band	Band max. (eV)	Peak cross section (Mb)	ΔE (eV)	f_0	Character
I	7.26	6.5	7.16	0.0093	$0.99n_O \rightarrow 3s$
II	7.80	16.6	7.49	0.0153	$0.98n_O \rightarrow 3p''$
			7.58	0.0147	$0.98n_O \rightarrow 3p'$
			7.74	0.0189	$0.98n_O \rightarrow 3p$
			7.88	0.0064	$0.97\sigma_{CO} \rightarrow 3s$
III	8.60	19.0	8.32	0.0096	$0.96\sigma_{CO} \rightarrow 3p'$
			8.36	0.0353	$0.92\sigma_{CO} \rightarrow 3p''$
			8.42	0.0148	$0.83n_O \rightarrow 3d$
			8.47	0.0024	$0.88\sigma_{CO} \rightarrow 3p$
			8.57	0.0044	$0.96n_O \rightarrow 3d'$
			8.60	0.0174	$0.98n_O \rightarrow 3d''$
			8.67	0.0036	$0.98n_O \rightarrow 3d'''$
IV	9.37	26.1	9.04	0.0068	$0.98n_{CO} \rightarrow$ Ryd-like(d)
			9.19	0.0247	$0.89\sigma_{CO} \rightarrow 3d$
			9.24	0.0080	$0.88n_O \rightarrow 4d$
			9.29	0.0129	$0.92\sigma_{CO} \rightarrow 3d/3p$
			9.38	0.0071	$0.89n_O \rightarrow 5s$
			9.40	0.0082	$0.93\sigma_{CO} \rightarrow 3d$
			9.49	0.0067	$0.90n_O \rightarrow 5p$
			9.54	0.0339	$0.64\sigma_{CO} \rightarrow 3d + 0.22\sigma_{CH/n_O} \rightarrow 3s$
			9.59	0.0033	$0.53n_O \rightarrow$ Ryd-like$+ 0.35\sigma_{CH/n_O} \rightarrow 3s$
			9.65	0.0348	$0.47n_O \rightarrow 5d + 0.27\sigma_{CH/n_O} \rightarrow 4s + 0.22\sigma_{CO} \rightarrow$ Ryd-like(d)
			9.70	0.0105	$0.93n_O \rightarrow 6s$

Table 2 Energy value (eV), quantum defect (δ), and tentative assignment of the Rydberg series converging to the ionic electronic ground, first and second excited states of propylene oxide

E_n	δ	Assignment	E_n	δ	Assignment
E_1 = 10.26 eV			E_2 = 11.23 eV		
7.15	0.91	3s	7.93	0.97	3s
8.73	1.02	4s	9.72	0.99	4s
7.80	0.65	3p	8.67	0.70	3p
7.94	0.58	3p′	8.73	0.66	3p′
8.08	0.50	3p″	8.80	0.63	3p″
9.05	0.64	4p	10.02	0.65	4p
9.14	0.52	4p′	10.07	0.57	4p′
9.20	0.42	4p″	10.09	0.54	4p″
8.45	0.26	3d	9.38	0.29	3d
8.50	0.22	3d′	9.47	0.24	3d′
8.56	0.17	3d″	9.52	0.18	3d″
E_3 = 12.88 eV					
9.45	1.01	3s			

Table 3 Proposed vibrational assignments in the 6.7–7.5 eV absorption band of propylene oxide (Band I). ΔE (in eV) represents the energy of one extra quantum in the vibrational progression

Energy (eV)	Assignment	$\Delta E(\upsilon'_{24})$	$\Delta E(\upsilon'_{23})$
7.10	0_0^0		
7.13	24_0^1	0.03	
7.15	24_0^2	0.02	
7.17[a]	24_0^3	0.02	
7.23			
7.26	24_0^1	0.03	
7.31			
7.35	23_0^1		0.04
7.40	23_0^2		0.04
7.44	23_0^3		0.04

[a] Broader.

our TDDFT calculations that places a $n_O \rightarrow 3s$ transition at 7.16 eV, with an oscillator strength of 0.01.

C.2. The 7.5–8.3 eV photon energy range (band II)

The second absorption band is defined between 7.5 and 8.3 eV, with the peak placed at 7.80 eV with a cross section of 16.6 Mb (Fig. 5). This band shows a different picture compared to the previous one (band I) with very pronounced and sharp features. These structures are signatures of Rydberg states, characterized by excitation into diffuse orbitals. We attribute this band to the fourth singlet excited state, $n_O \rightarrow 3p$ with an oscillator strength of 0.0189, whereas the $n_O \rightarrow 3p'$ (f_0 = 0.0153) and $n_O \rightarrow 3p$ (f_0 = 0.0147) should also contribute to the band pattern. In Fig. 2 a red shift of 0.23 eV of the band maximum peak is observed for the theoretical calculations compared to experimental results. Additionally, we have identified the 3p Rydberg series converging to the IE_1 state starting at 7.80 eV, guided by the quantum defect calculations (Table 2), and aided by the excited states assignments involving Rydberg character orbitals as predicted by the quantum chemical calculations. We also observed features which we tentatively assigned to two different vibrational progressions (Table 4). One associated with the υ_{22} CH_3 bending with an average value of 0.055 eV, while the other could be assigned to υ_{14} CH bending or υ_{15} CH_2 wagging, with a consistent spacing of 0.14 eV, according to Barone *et al.*[22] These

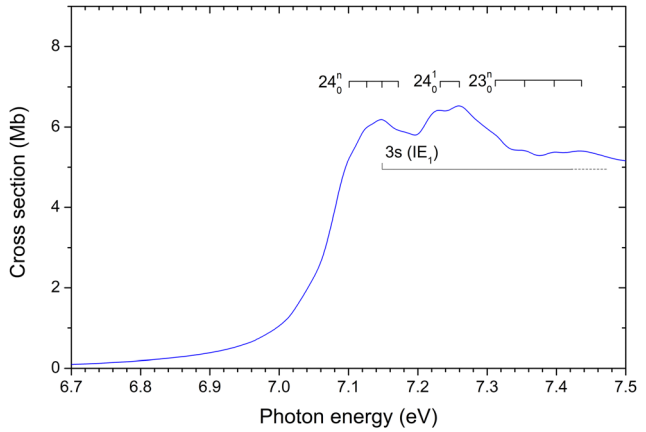

Fig. 4 Vibrational progressions and Rydberg series in the 6.7–7.5 eV energy range of the absorption band I of propylene oxide.

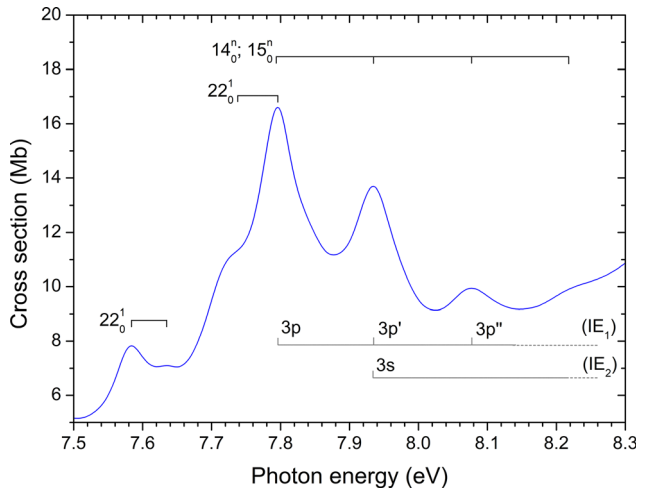

Fig. 5 Vibrational progressions and Rydberg series in the 7.5–8.3 eV energy range of absorption band II of propylene oxide.

Table 4 Proposed vibrational assignments in the 7.5–8.3 eV absorption band of propylene oxide (band II). ΔE (in eV) represents the energy of one extra quantum in the vibrational progression. The symbol ";" means alternative assignments

Energy (eV)	Assignment	$\Delta E(\upsilon'_{22})$	$\Delta E(\upsilon'_{14};\upsilon'_{15})$
7.58	0^0_0		
7.63	22^1_0	0.05	
7.74			
7.80	22^1_0	0.06	
7.94	$14^1_0;15^1_0$		0.14
8.08	$14^2_0;15^2_0$		0.14
8.22	$14^3_0;15^3_0$		0.14

assignments are in accordance with the orbitals involved in these electronic excitations (Fig. 3). The 0–0 origin band is observed at 7.58 eV. Again, there is a fairly good agreement between our results and those shown by Breest *et al.*[36] for band II, where they have identified two $n_O \rightarrow R(3p)$ excited states peaking at 7.70 eV and 7.85 eV. On the other hand, the major difference lies in the assignments for vibrational modes involved in this absorption band, since the authors assumed methyl rocking mode with 1070 cm^{-1} frequency. This difference is likely due to the better resolution of our measurements compared to those by Breest *et al.*[36] The spectral resolution of Cohen *et al.*[37] does not allow to distinguish the fine structures observed in this absorption band. Even so, they also assign this to a $n_O \rightarrow R(3p)$ transition, peaked at 7.75 eV, which is a redshift of 0.05 eV compared to our results.

C.3. The 8.3–9.0 eV photon energy range (band III)

Between 8.3 and 9.0 eV photon energy, we can find the third absorption band, peaking at 8.60 eV (19 Mb), assigned to a $n_O \rightarrow 3d''$ electronic transition, with an oscillator strength of 0.017 (Table 1). At lower energy a pronounced peak at 8.45 eV with a 17.7 Mb cross-section is observed and attributed to a $\sigma_{CO} \rightarrow 3p''$ excitation with a stronger oscillator strength of 0.035. Due to the better resolution as compared to Breest *et al.*[36], fine and well-defined structures are observed for this band. An inspection of Table 1 shows several excited states for this absorption band, mainly assigned to transitions from the n_O occupied orbital to a component of a d-type Rydberg-like orbital, and from the occupied σ_{CO} to some component of the 3p Rydberg-like orbital. The agreement between experimental and theoretical calculations is quite good with a difference of 0.22 eV in the maximum peak, as shown in Fig. 2. Indeed, this discrepancy is consistent across the spectrum, for all absorption bands excluding band I.

The Rydberg series determination, mainly based on the quantum defect values, indicates a 3d Rydberg series starting at 8.448 eV (δ = 0.26), converging to the IE_1 state, as shown in Fig. 6 and listed in Table 2. These results are in accordance with the transition assignments for this energy range predicted by quantum chemical calculations, as shown in Table 1. We have also tentatively attributed vibrational assignments to some

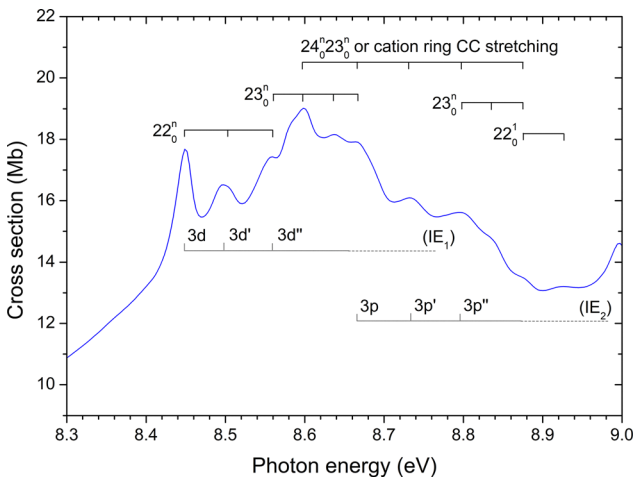

Fig. 6 Vibrational progressions and Rydberg series in the 8.3–9.0 eV energy range of absorption band III of propylene oxide.

Table 5 Proposed vibrational assignments in the 8.3–9.0 eV absorption band of propylene oxide (band III). ΔE (in eV) represents the energy of one extra quantum in the vibrational progression

Energy (eV)	Assignment	$\Delta E(\upsilon'_{22})$	$\Delta E(\upsilon'_{23})$	$\Delta E(\upsilon'_{23}\upsilon'_{24})$ or cation ring CC stretching
8.45	0_0^0			
8.50	22_0^1	0.05		
8.56	22_0^2	0.06		
8.60	23_0^1		0.04	
8.64	23_0^2		0.04	
8.67	$23_0^3/23_0^124_0^1$		0.03	0.07
8.73	$23_0^224_0^2$			0.06
8.80	$23_0^324_0^3$			0.07
8.84	$23_0^1/23_0^424_0^4$	0.04	0.08	
8.88	23_0^2		0.04	
8.93	22_0^1	0.05		

features observed in this band, namely υ_{22} and υ_{23}, both involving bending of the methyl group. Furthermore, a vibrational progression with average spacing of 0.07 eV (564.6 cm^{-1}) is also depicted. Since there is no vibrational mode experimentally or theoretically predicted for this vibration frequency, we tentatively assigned this progression to a combination of the υ_{23} and υ_{24} vibrational modes, which results in a frequency of 575 cm^{-1} (Table 5). Additional calculations were also carried out to check the contribution of vibrational modes of the cation ground state, as presented in Table S5. In fact, the calculations show a ring CC stretching mode at 630.1 cm^{-1} frequency, which is quite close to our results, suggesting the involvement of this vibrational mode as a strong possibility.

C.4. The 9.0–10.8 eV photon energy range (band IV)

The results for band IV between 9.0 and 10.8 eV are shown in Fig. 7. The measured spectrum of propylene oxide in this energy region is quite rich, with narrow features very close in energy. There are some features that stand out including the peaks at 9.37 eV, 9.52 eV, 9.68 eV and 10.2 eV, with the highest cross section value (44.2 Mb). The many excited states in this energy range are related to electronic transitions from lower energies occupied molecular orbitals, such as, HOMO−1, HOMO−2 and HOMO−3, to higher unoccupied molecular orbitals as predicted by quantum chemical calculations (Table 1). Looking at Fig. 2, we can see that the theoretical calculations produce cross sections in overall close agreement with experiments as far as the magnitude is concerned, with energies deviating between 0.15 eV and 0.25 eV. We have tentatively assigned some structures to vibrational progressions which are superimposed on the different Rydberg series converging to IE_1 and IE_2 identified in this absorption band. The υ_{22} CH_3 bending and υ_{24} CH_3 torsion were identified, as well as

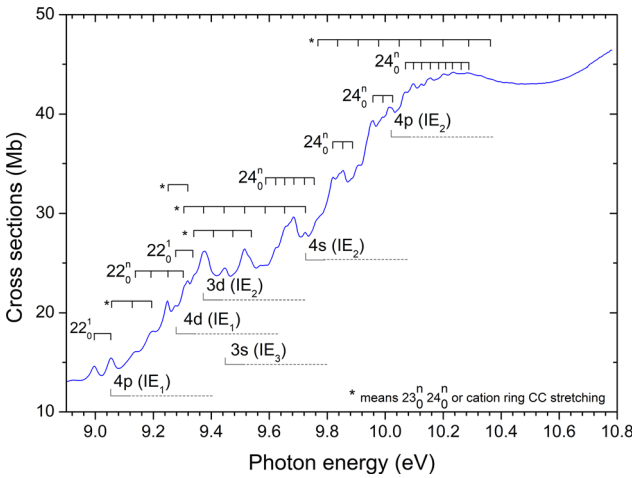

Fig. 7 Vibrational progressions and Rydberg series in the 9.0–10.8 eV energy range of absorption band IV of propylene oxide. The notation "*" means $23_0^n24_0^n$ vibrational mode or cation ring CC stretching.

Table 6 Proposed vibrational assignments in the 9.0–10.8 eV absorption band of propylene oxide (band IV). ΔE (in eV) represents the energy of one extra quantum in the vibrational progression

Energy (eV)	Assignment	$\Delta E(\upsilon'_{22})$	$\Delta E(\upsilon'_{24})$	$\Delta E(\upsilon'_{23}\upsilon'_{24})$ or cation ring CC stretching
9.00	0_0^0			
9.05	22_0^1	0.05		
9.14				
9.20	22_0^1	0.06		
9.25	22_0^2	0.06		
9.28	$23_0^124_0^1$			0.08
9.31	22_0^3	0.05		
9.32	$23_0^124_0^1$			0.07
9.34	22_0^1	0.06		
9.38	$23_0^124_0^1$			0.07
9.40	$23_0^124_0^1$			0.06
9.45	$23_0^224_0^2$			0.07
9.47	$23_0^224_0^2$			0.07
9.52	$23_0^224_0^2$			0.07
9.54	$23_0^324_0^3$			0.07
9.59	$23_0^324_0^3$			0.07
9.62	24_0^1		0.03	
9.65	$24_0^2/23_0^424_0^4$	0.03	0.06	
9.68	24_0^3		0.03	
9.72	$24_0^4/23_0^524_0^5$	0.04	0.07	
9.76	24_0^5		0.04	
9.77				
9.82				
9.84	$23_0^124_0^1$			0.07
9.86	24_0^1		0.04	
9.88	24_0^2		0.04	
9.91	$23_0^224_0^2$			0.07
9.96				
9.98	$23_0^324_0^3$			0.07
9.99	24_0^1		0.03	
10.03	24_0^2		0.04	
10.05	$23_0^424_0^4$			0.07
10.07				
10.10	24_0^1		0.03	
10.12	$24_0^2/23_0^524_0^5$	0.02	0.07	
10.16	24_0^3		0.04	
10.18	24_0^4		0.02	
10.20	$24_0^5/23_0^624_0^6$	0.02	0.06	
10.21				
10.23	24_0^6		0.03	
10.26	24_0^7		0.03	
10.28	$24_0^8/23_0^724_0^7$	0.02	0.08	
10.37	$23_0^824_0^8$			0.09

a progression which could be related to a combination of υ_{23} and υ_{24} vibrational modes or associated with the ring CC stretching of the cation, similar to that observed in band III (Table 6).

C.5. The potential energy curves for C–CH_3 stretching

The calculated potential energy curves (PECs) for the eight lowest excited states along the C–CH_3 bond stretching coordinate, obtained at the TDDFT/CAMB3LYP/aug-cc-pVQZ level, are shown in Fig. 8. The C–CH_3 stretching coordinate was selected as a representative nuclear displacement to probe the sensitivity of the low-lying excited states to molecular distortion and to investigate the evolution of their electronic character upon bond elongation. The purpose of this analysis is not to identify the dominant photodissociation pathway of propylene oxide, but rather to provide insight into the coupling between Rydberg and valence states and its role in shaping the excited-state landscape accessed in the VUV region.

The overall behaviour of the curves shows that most of the states have a predominantly Rydberg character considering small displacements (<0.3 Å) near the C–CH_3 equilibrium length (at around 1.5 Å). This is consistent with the NTO analysis discussed above, in which these low-lying excited states are mainly characterized by transitions from the n_O and σ_{CO} orbitals to diffuse Rydberg-like orbitals. As the bond is further stretched, most of the excited states evolve into dissociative profiles, indicating that the C–CH_3 bond stretch progressively weakens their dominant Rydberg character and favours mixing with valence σ^* orbitals. This is particularly evident for the first excited state, for which the MO character was followed along the stretching coordinate and is shown at selected C–CH_3 distances in the same figure. At the equilibrium geometry, the first excited state was assigned as having Rydberg character ($n_O \rightarrow 3s$). Around 2 Å, however, this state shows mixed Rydberg-valence nature ($3s/\sigma^*$), and finally, at larger displacements, the virtual orbital becomes predominantly σ^* valence. This clearly shows a Rydberg-to-valence behavior for this excited state.

Additional one-dimensional potential energy scans along the C–O stretching coordinates are reported in the SI and are intended solely as qualitative diagnostics of excited-state evolution upon bond elongation.

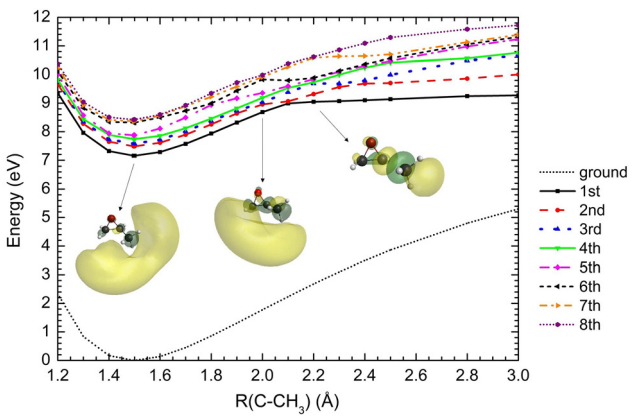

Fig. 8 Potential energy curves of the eight lowest singlet excited states of propylene oxide along the C–CH stretch.

D. Conclusions

In this work we have presented a comprehensive experimental and theoretical study of the electronic excited states of propylene oxide. The experimental absolute photoabsorption cross-sections, in the 6–11 eV energy range, were assigned with the support of theoretical calculations obtained at the TDDFT/CAMB3LYP/aug-cc-pVQZ level. The computed vertical excitation energies and oscillator strengths reproduce the main features of the experimental spectrum, enabling reliable assignment of the observed absorption bands. NTO analysis revealed a predominance of transitions initiated in the n_O and σ orbitals into diffuse Rydberg-like orbitals of s, p and d-type.

The fine structure of the measured spectrum was assigned to vibronic excitations involving the methyl group: CH_3 bending (υ_{22} and υ_{23}) and CH_3 torsion (υ_{24}). We have also reported a vibrational progression which may be related to the cation ring CC stretching with an average frequency of about 565 cm^{-1}. Additionally, we have obtained potential energy curves for the low-lying excited states along the C–CH_3 stretching coordinate, at the same level of theory. The PECs reveal that the initially Rydberg states evolve into dissociative states at larger bond distances as σ^* valence character increases. This Rydberg-to-valence crossover suggests that vibrational distortion may enhance coupling to dissociative states and facilitate photodissociation pathways. Overall, the close agreement between experiment and theory strengthens the electronic-structure assignment and provides new insight into the excited-state dynamics of propylene oxide in the VUV region.

Author contributions

Conceptualization: M. M. and A. S. B.; data curation: N. C. J.; funding acquisition: M. M., A. S. B., F. F. S., N. C. J. and S. V. H.; methodology: J. A. F. F. S., N. C. J. and A. S. B.; resources: N. C. J., S. V. H.; writing – original draft: M. M. and A. S. B.; writing – review & editing: F. F. S., N. C. J., S. V. H., D. S. and R. R.

Conflicts of interest

There are no conflicts to declare.

Data availability

Data for this article, including experimental cross-sections and theoretical cross-sections obtained with the vertical approximation based in the TDDFT/CAMB3LYP/aug-cc-pVQZ calculation, ground state frequencies of propylene oxide and the propylene oxide cation as well as calculated vertical excitation energies and oscillator strengths obtained at TDDFT/CAMB3LYP/aug-cc-pVQZ, TDDFT/CAMB3LYP/aug-cc-pVTZ, and

TDDFT/B3LYP/aug-cc-pVTZ levels of theory are available at Zenodo at https://doi.org/10.5281/zenodo.18161967.

The supplementary information (SI) describes the optimized molecular geometry for propylene oxide, obtained at the DFT/CAMB3LYP/aug-cc-pVQZ level of theory. See DOI: https://doi.org/10.1039/d6cp00031b.

Acknowledgements

R. R., M. M., J. A. and F. F. D. S. acknowledge the Portuguese National Funding Agency FCT-MCTES through the research grant number UID/FIS/00068/2025 (CEFITEC). M. M. acknowledges FCT through the research grant 2023.14518.PEX (https://doi.org/10.54499/2023.14518.PEX), and F. F. D. S. acknowledges the BIOSPHERE project and the FCTMobility grant FCT/Mobility/1309167586/2024-25. The project 21GRD02 BIOSPHERE has received funding from the European Partnership on Metrology (Funder ID: 10.13039/100019599), cofinanced by the European Union's Horizon Europe Research and Innovation Programme and by the Participating States. The research leading to this result has been supported by the project CALIPSOplus under the Grant Agreement 730872 from the EU Framework Programme for Research and Innovation HORIZON 2020. ASB acknowledges financial support from the Brazilian agency Conselho Nacional de Desenvolvimento Científico e Tecnológico (CNPq) and computational support from Professor Carlos A. M. de Carvalho at LFTC-DFis-UFPR and at LCPAD-UFPR.

References

1 Vladimir Prelog, Chirality in Chemistry, Nobel Lecture, 1975, preprint.
2 M. G. Weller, The Mystery of Homochirality on Earth, *Life*, 2024, **14**, 341.
3 S. Pizzarello and T. L. Groy, Molecular asymmetry in extraterrestrial organic chemistry: an analytical perspective, *Geochim. Cosmochim. Acta*, 2011, **75**, 645–656.
4 Q. Sallembien, L. Bouteiller, J. Crassous and M. Raynal, Possible chemical and physical scenarios towards biological homochirality, *Chem. Soc. Rev.*, 2022, **51**, 3436–3476.
5 C. R. Arumainayagam, R. T. Garrod, M. C. Boyer, A. K. Hay, S. T. Bao, J. S. Campbell, J. Wang, C. M. Nowak, M. R. Arumainayagam and P. J. Hodge, Extraterrestrial prebiotic molecules: photochemistry vs. radiation chemistry of interstellar ices, *Chem. Soc. Rev.*, 2019, **48**, 2293–2314.
6 A. Bergantini, M. J. Abplanalp, P. Pokhilko, A. I. Krylov, C. N. Shingledecker, E. Herbst and R. I. Kaiser, A combined experimental and theoretical study on the formation of interstellar C_3H isomers, *Science*, 1996, **274**, 1508–1511.
7 Q. T. Wu, H. Anderson, A. K. Watkins, D. Arora, K. Barnes, M. Padovani, C. N. Shingledecker, C. R. Arumainayagam and J. B. R. Battat, Role of Low-Energy (<20 eV) Secondary Electrons in the Extraterrestrial Synthesis of Prebiotic Molecules, *ACS Earth Space Chem.*, 2024, **8**, 79–88.
8 M. Tia, B. Cunha De Miranda, S. Daly, F. Gaie-Levrel, G. A. Garcia, I. Powis and L. Nahon, Chiral asymmetry in the photoionization of gas-phase amino-acid alanine at lyman-α radiation wavelength, *J. Phys. Chem. Lett.*, 2013, **4**, 2698–2704.
9 C. Meinert, S. V. Hoffmann, P. Cassam-Chenaï, A. C. Evans, C. Giri, L. Nahon and U. J. Meierhenrich, Photonenergy-controlled symmetry breaking with circularly polarized light, *Angew. Chem., Int. Ed.*, 2014, **53**, 210–214.
10 J. J. Flores, W. A. Bonner and G. A. Massey, Asymmetric Photolysis of (RS)-Leucine with Circularly Polarized Ultraviolet Light, *J. Am. Chem. Soc.*, 1977, **99**, 3622–3625.
11 U. J. Meierhenrich, J. J. Filippi, C. Meinert, S. V. Hoffmann, J. H. Bredehöft and L. Nahon, Photolysis of rac-leucine with circularly polarized synchrotron radiation, *Chem. Biodivers.*, 2010, **7**, 1651–1659.
12 F. F. da Silva, P. Bartl, S. Denifl, T. D. Märk, A. M. Ellis and P. Scheier, Formation of the magic L-serine octamer in helium nanodroplets, *ChemPhysChem*, 2010, **11**, 90–92.
13 B. A. McGuire, P. Brandon Carroll, R. A. Loomis, I. A. Finneran, P. R. Jewell, A. J. Remijan and G. A. Blake, Discovery of the interstellar chiral molecule propylene oxide (CH_3CHCH_2O), *Science*, 2016, **352**, 1449–1452.
14 E. J. Gallegos and R. W. Kiser, Electron Impact Spectroscopy of Ethylene Oxide and Propylene Oxide, *J. Am. Chem. Soc.*, 1961, **83**, 773–777.
15 R. Rodrigues, D. Bou Debes, M. Mendes, P. Guerra, G. Mestre, S. Eden, L. M. Cornetta, O. Ingólfsson and F. F. da Silva, Experimental and Theoretical Study on Electron Ionization and Fragmentation of Propylene Oxide—the First Chiral Molecule Detected in the Interstellar Medium, *J. Phys. Chem. A*, 2024, **128**, 4795–4805.
16 F. Liu, L. Sheng, F. Qi, H. Gao, C. Li, Y. Zhang, S. Yu, K. C. Lau and W. K. Li, A Vacuum Ultraviolet Photoionization Mass Spectrometric Study of Propylene Oxide in the Photon Energy Region of 10–40 eV, *J. Phys. Chem. A*, 1999, **103**, 8179–8186.
17 R. Bombach, J.-P. Stadelmann and J. Volt, Unimolecular dissociations of excited $C_3H_6O^+$: a comparative photoelectron-photoion coincidence study of 2-epoxypropane and acetone, *Chem. Phys.*, 1982, **72**, 259–266.
18 E. J. McAlduff and K. N. Houk, Photoelectron spectra of substituted oxiranes and thiiranes. Substituent effects on ionization potentials involving σ orbitals, *Can. J. Chem.*, 1977, **55**, 318–332.
19 K. Watanabe, Ionization potentials of some molecules, *J. Chem. Phys.*, 1957, **26**, 542–547.
20 M. C. Tobin, The infrared spectrum of propylene oxide, *Spectrochim. Acta*, 1960, **16**, 1108–1110.
21 P. L. Polavarapu, B. A. Hess and L. J. Schaad, Vibrational spectra of epoxypropane, *J. Chem. Phys.*, 1984, **82**, 1705–1710.
22 V. Barone, M. Biczysko, J. Bloino and C. Puzzarini, Accurate molecular structures and infrared spectra of trans-2,3-dideuterooxirane, methyloxirane, and trans-2,3-dimethyloxirane, *J. Chem. Phys.*, 2014, **141**, 034107.

23 K. Vavra, E. Doring, J. Jakob, F. Peterß, M. Kaufmann, P. Stahl, T. F. Giesen and G. W. Fuchs, High-resolution infrared spectra and rovibrational analysis of the ν_{12} band of propylene oxide, *Phys. Chem. Chem. Phys.*, 2024, **26**, 23886–23892.
24 C. Merten, J. Bloino, V. Barone and Y. Xu, Anharmonicity effects in the vibrational CD spectra of propylene oxide, *J. Phys. Chem. Lett.*, 2013, **4**, 3424–3428.
25 A. D. Garcia, J. Topin, J. Bocková, N. C. Jones, S. V. Hoffmann and C. Meinert, Chiroptical activity of gas-phase propylene oxide predicting the handedness of interstellar circular polarization in the presolar nebula, *Sci. Adv.*, 2022, **8**(46), eadd4614.
26 J. D. Swalen and D. R. Herschbach, Internal barrier of propylene oxide from the microwave spectrum. I, *J. Chem. Phys.*, 1957, **27**, 100–108.
27 S. Stranges, S. Turchini, M. Alagia, G. Alberti, G. Contini, P. Decleva, G. Fronzoni, M. Stener, N. Zema and T. Prosperi, Valence photoionization dynamics in circular dichroism of chiral free molecules: the methyl-oxirane, *J. Chem. Phys.*, 2005, **122**, 244303.
28 S. Turchini, N. Zema, G. Contini, G. Alberti, M. Alagia, S. Stranges, G. Fronzoni, M. Stener, P. Decleva and T. Prosperi, Circular dichroism in photoelectron spectroscopy of free chiral molecules: experiment and theory on methyl-oxirane, *Phys. Rev. A: At., Mol., Opt. Phys.*, 2004, **70**, 014502.
29 M. Hodecker, M. Biczysko, A. Dreuw and V. Barone, Simulation of Vacuum UV Absorption and Electronic Circular Dichroism Spectra of Methyl Oxirane: The Role of Vibrational Effects, *J. Chem. Theory Comput.*, 2016, **12**, 2820–2833.
30 S. Luber, M. Iannuzzi and J. Hutter, Raman spectra from ab initio molecular dynamics and its application to liquid *S*-methyloxirane, *J. Chem. Phys.*, 2014, **141**, 094503.
31 M. Elango, G. S. MacIel, F. Palazzetti, A. Lombardi and V. Aquilanti, Quantum chemistry of C3H6O molecules: Structure and stability, isomerization pathways, and chirality changing mechanisms, *J. Phys. Chem. A*, 2010, **114**, 9864–9874.
32 T. D. Crawford and K. Ruud, Coupled-Cluster Calculations of Vibrational Raman Optical Activity Spectra, *ChemPhysChem.*, 2011, **12**, 3442–3448.
33 P. Stahl, B. E. Arenas, O. Zingsheim, M. Schnell, L. Margulès, R. A. Motiyenko, G. W. Fuchs and T. F. Giesen, Deciphering the rotational spectrum of the first excited torsional state of propylene oxide, *J. Mol. Spectrosc.*, 2021, **378**, 111445.
34 M. A. Lowe, J. S. Alper, R. Kawiecki and P. J. Stephens, Scaled ab initio force fields for ethylene oxide and propylene oxide, *J. Phys. Chem.*, 1986, **90**, 41–50.
35 M. Stener, G. Fronzoni, D. Di Tommaso and P. Decleva, Density functional study on the circular dichroism of photoelectron angular distribution from chiral derivatives of oxirane, *J. Chem. Phys.*, 2004, **120**, 3284–3296.
36 A. Breest, P. Ochmann, F. Pulm, K. H. Godderz, M. Carnell and J. Hormes, Experimental circular dichroism and vuv spectra of substituted oxiranes and thiiranes, *Mol. Phys.*, 1994, **82**, 539–551.
37 D. Cohen, M. Levi, H. Bas and A. Gedanken, Excited Electronic States of Optically Active Substituted Ethylene Oxides: (−)-(*S*)-2-Methyloxirane and (−)-(*S*,*S*)-2,3-Dimethyloxirane, *J. Am. Chem. Soc.*, 1983, **105**, 1738–1742.
38 D. Duflot, N. C. Hoffmann, S. Vrønning Jones and P. Limão-Vieira, in *Radiation in Bioanalysis: Spectroscopic Techniques and Theoretical Methods, BIOANALYSIS*, ed. A. S. Pereira, P. Tavares and P. Limão-Vieira, Springer International Publishing, 2019, vol. 8, pp. 43–81.
39 G. M. J. Barca, C. Bertoni, L. Carrington, D. Datta, N. De Silva, J. E. Deustua, D. G. Fedorov, J. R. Gour, A. O. Gunina, E. Guidez, T. Harville, S. Irle, J. Ivanic, K. Kowalski, S. S. Leang, H. Li, W. Li, J. J. Lutz, I. Magoulas, J. Mato, V. Mironov, H. Nakata, B. Q. Pham, P. Piecuch, D. Poole, S. R. Pruitt, A. P. Rendell, L. B. Roskop, K. Ruedenberg, T. Sattasathuchana, M. W. Schmidt, J. Shen, L. Slipchenko, M. Sosonkina, V. Sundriyal, A. Tiwari, J. L. Galvez Vallejo, B. Westheimer, M. Włoch, P. Xu, F. Zahariev and M. S. Gordon, Recent developments in the general atomic and molecular electronic structure system, *J. Chem. Phys.*, 2020, **152**, 154102.